CrystEngComm

Accepted Manuscript

ROYAL SOCIETY OF CHEMISTRY

www.rsc.org/crystengcomm

Journal Name

ARTICLE

Synthesis of Hierarchical ZnO/$ZnFe_2O_4$ Nanoforest with Enhanced Gas-sensing Performance toward Ethanol

Received 00th January 20xx,
Accepted 00th January 20xx

DOI: 10.1039/x0xx00000x

www.rsc.org/

Jian Ma †, Yaxin Cai †, Xiaowei Li, Shiting Yao, Yang Liu, Fengmin Liu*, Geyu Lu*

Hierarchical ZnO/$ZnFe_2O_4$ nanoforest with ZnO backbones and $ZnFe_2O_4$ nanosheets were successfully prepared by a facile two-step process. The products were fabricated through immersing the as-synthesized ZnO nanorod arrays in 0.2M aqueous solution of ferrous sulfate and subsequent calcination at 500℃. Various techniques were employed for the characterization of the structure and morphology of the hybrid nanostructures. The results showed that high density of $ZnFe_2O_4$ nanosheets were planted on the surface of ZnO nanorods. Interestingly, the morphologies of ZnO/$ZnFe_2O_4$ hierarchical nanostructures can be tailored by changing the concentration of $FeSO_4$ solution and the immersion time. A possible formation process and growth mechanism was proposed as the ZnO nanorods were partly dissolved dring the immersion period. In order to demonstrate the potential application, two sensors based on the bare ZnO and ZnO/$ZnFe_2O_4$ composites were fabricated and their gas sensing properties were investigated. The results indicated that the obtained advanced ZnO/$ZnFe_2O_4$ nanostructures exhibited enhanced sensing properties to ethanol compared to primary ZnO nanorods. For example, upon exposure to 100 ppm ethanol, the response of hierarchical ZnO/$ZnFe_2O_4$ composites was about 4 times higher than that of primary ZnO nanorods at the operating temperature of 275°C.

1. Introduction

Hetero-nanostructures characterized by two or more metal oxides have attracted growing attentions due to their great potential applications in gas sensor, [1–3] catalysis, [4] and lithium-ion battery. [5] In recent years, many studies have demonstrated that the performance of these composites are much brilliant compared to their individual metal oxide counterparts.[6-9] Therefore, great progress has been made in the synthesis of these hybrid composites with different components nanostructures and numerous hetero-nanostructures have been achieved, such as α-Fe_2O_3/SnO_2, [10] ZnO/TiO_2,[11] ZnO/In_2O_3,[12] α-Fe_2O_3/ZnO[13] and SnO_2/ZnO.[14-15] Among various metal oxide, ZnO, known as a famous wide-band semiconductor (3.37 eV), has always been the research hotspot in the field of materials. Meanwhile, the binary oxide semiconductors, such as spinel ferrites (AFe_2O_4, A = Zn, Ni, Cu, Cd, Co), have also attracted tremendous attention because of their potential application in gas sensors. Considering the fact that the enhanced performances can be obtained by assembling the individual metal oxide together, ZnO/$ZnFe_2O_4$ composites with hierarchical architectures may bring some potential properties.[16-18] For this reason, design and synthesis ZnO/$ZnFe_2O_4$ composites with novel architectures still have importantly scientific and practical significance.

In virtue of the advance in nanoscience, various nanostructured oxide semiconductors have been prepared in recent years. [19–21] Especially, 1D nanostructured materials was extensively prepared as templates due to its structural versatility, easy fabrication and highly self-assembled. Besides, although great progress has been made on the synthesis approaches for 1 D nanostructure, there still remains a great challenge to develop a facile, mild, and low cost method for the preparation of such nanostructures. Compared to other kinds of methods, ultrasonic spray pyrolysis (USP) has many advantages, such as effective stoichiometry control, excellent homogeneity, relatively low processing temperature and low cost fabrication for large area film. [22-23]

In this paper, we successfully prepared ZnO/$ZnFe_2O_4$ hybrid nanostructures by a facile two-step method. Firstly, ordered ZnO nanorod arrays were pre-prepared on FTO (Fluorine-doped tin oxide) glass substrates by USP process. Subsequently, the ZnO nanorod arrays used as the template were immersed in the solution of $FeSO_4$ for a certain time. (Scheme 1) The template was partially dissolved by H^+ produced from $FeSO_4$ hydrolysis, which in turn accelerated the hydrolysis and acted as a crucial step initiating the construction of the architecture. The formation mechanism of the ZnO/$ZnFe_2O_4$ nanoforest was discussed and the influence of the Fe^{2+} concentration on the morphologies of the ZnO/$ZnFe_2O_4$ products has been investigated. In order to demonstrate the potential applications, the resulting composite was used to fabricate gas sensors. It was found that the gas sensor based on as-prepared ZnO/$ZnFe_2O_4$

Address: State Key Laboratory on Integrated Optoelectronics, College of Electronic Science and Engineering, Jilin University, Changchun, 130012, People's Republic of China. † These authors contributed equally to this work. Correspondence and requests for materials should be addressed to F. Liu (email: liufm@jlu.edu.cn) or to G. Lu (email: lugy@jlu.edu.cn). Fax: +86 431 85167808; Tel: +86 431 85167808;

semiconductor composites showed a high response to ethanol at 275°C, superior to the bare ZnO nanorods. The enhanced performance may be attributed to the unique structure as well as the change of the heterojunction barrier at different gas atmosphere.

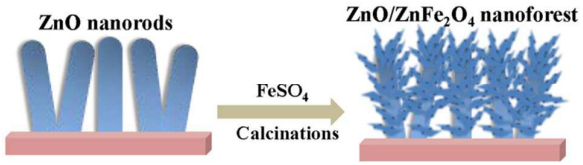

Scheme1 Illustration for the fabrication of hierarchical $ZnO/ZnFe_2O_4$ nanoforest.

2. Experimental details

2.1 Synthesis of $ZnO/ZnFe_2O_4$ hierarchical nanostructures

All chemicals in the experiment were analytical reagent grade and used without further purification. The $ZnO/ZnFe_2O_4$ hierarchical nanostructures were prepared by a facile two-step method. Firstly, ZnO nanorod arrays were synthesized by a seed-assisted chemical reaction as described in our previous report.[24] In a typical synthesis process, 0.9 mmol zinc acetate dihydrate ($Zn(CH_3COO)_2 \bullet 2H_2O$) and 1.5 mmol hexamethylenetetramine (HMT) were dissolved in 10mL deionized water by magnetic stirring for 30 min at room temperature. Then the prepared mixture as the precursor solution was sprayed by a general ultrasonic generator for 10 min at 300°C. As a result, ZnO seed layer was preferentially deposited on the FTO substrate. Subsequently, the precursor with the mixture of 10 mmol zinc chloride ($ZnCl_2$) and 0.1 mL monoethanolamine was sprayed on- to the seed coated FTO for 2 h at 300°C. Then the obtained products were treated by sintering at 500°C for 2 h. Secondly, the FTO glass with ZnO nanorod arrays was immersed in 0.1-0.8 M aqueous solutions of ferrous sulphate ($FeSO_4$) for 5-30 min, the solution-immersion conditions are summarized in Table 1. After being washed with deionized water and dried at 80°C, the resulting films were subjected to calcination at 500°C in air atmosphere.

Table1 Solution-immersion conditions for the fabrication of $ZnO/ZnFe_2O_4$ nanostructured films

Sample No.	Concentration of $FeSO_4$ solution	Immersion time/min
S1	0.1M	30
S2	0.2M	30
S3	0.4M	30
S4	0.8M	30
S5	0.2M	5
S6	0.2M	10
S7	0.2M	20

2.2 Characterization of samples

The X-ray diffraction (XRD) patterns were recorded by a Rigaku D/max 2500 with Cu-Ka radiation (λ=0.15406nm) in the range of 20°-80° (2θ) at room temperature. Field emission scanning electron microscopy (FESEM) images were obtained using a JEOL JSM-7500F microscope with an acceleration voltage of 15 kV. The X-ray photoelectron spectroscopy (XPS) spectra was recorded on a Kratos ASIS-HS X-ray photoelectron spectroscope equipped with a standard and monochromatic source (Al KR) operated at 150 W (15 kV, 10 mA). Transmission electron microscopic (TEM) and high-resolution transmission electron microscopic (HRTEM) images were obtained on a JEOL JEM-3010 microscope operated at 200 kV, respectively. The energy dispersive X-ray spectroscopy (EDS) result was measured by the TEM attachment.

2.3 Fabrication and measurement of gas sensor

Gas sensors were fabricated as follows: the as-prepared products were scraped off from the glasses and subsequently dispersed in the deionized water to form a paste, and then coated on a ceramic tube (4 mm in length, 1.2 mm in external diameter, and 0.8 mm in internal diameter, attached with a pair of gold electrodes) by a small brush to form a thick film. A pair of electrodes was installed at each end of the alumina tube, and each electrode was connected with a Pt wire. Prior to the test, a Ni-Cr resistor was inserted into the ceramic tube as a heater, which allows for the control of the working temperature. The detail of the sensor fabrication and the testing process were described in our previous work.[25] The gas response S is defined as S=Ra/Rg, where Ra and Rg are the resistances of sensors in air and the target gas. The response and recovery times are defined as the time taken by the sensor to achieve 90% of the total resistance change in the case of adsorption and desorption, respectively.

3. Results and discussion

Fig.1a-b shows the FESEM image of the pure ZnO nanorods grown for 2h. A panoramic FESEM image was shown in Fig. 1a, from which a number of uniform nanorods were clearly observed. It can be observed from the enlarged FESEM image (Fig. 1b) that the ZnO nanorods have a smooth surface with a top diameter of about 500 nm. Fig.1c presents the SEM image of $ZnO/ZnFe_2O_4$ hierarchical nanostructures (S2 in Table1) prepared by immersing the pure ZnO in 0.2 M ferrous sulfate for 30 min. It can be seen that the uniform $ZnO/ZnFe_2O_4$ nanoforest were observed. No other morphologies can be detected, indicating a high yield of these nanostructures. The enlarged SEM image (Fig.1d) shows that lots of $ZnFe_2O_4$ nanosheets were attached on the surface of ZnO nanorods. After the $ZnFe_2O_4$ growth, the diameter of the nanorods was smaller than the original ones and about 300nm.

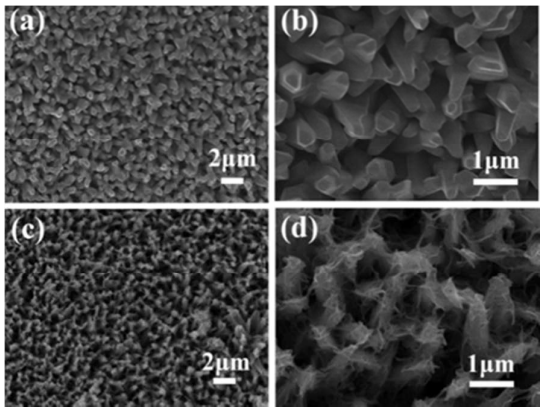

Fig. 1 FESEM images of (a, b) bare ZnO nanorods and (c, d) the $ZnO/ZnFe_2O_4$ nanoforest (S2)

The crystal structure and phase purity of the final products were identified by powder X-ray diffraction (XRD). Fig. 2 shows the typical XRD patterns of the pure ZnO nanorods (red curve) and as-synthesized $ZnO/ZnFe_2O_4$ hierarchical architectures (black curve) prepared after immersing ZnO nanorods in 0.2M ferrous sulfate for 30min. It can be seen that all diffraction peaks in the red curve can be well indexed to a hexagonal wurtzite structure of zinc oxide (JCPDS File No. 36-1451). After the Fe-contain layer was deposited, the peaks ascribed to FTO substrate appeared in the XRD pattern, which means that the ZnO nanorods were partly dissolved. The inset of Fig. 2 is the detail view of the XRD patterns from 20 to 50 degree. From the inset of Fig. 2, the diffraction peaks of the composites display a mixed crystal phases of ZnO and $ZnFe_2O_4$ (JCPDS File No. 89-1010). By contrast, the peaks of $ZnFe_2O_4$ were weaker than those of ZnO in the composite, probably because of the large content of ZnO in the sample. The result demonstrates the product is a mixture of ZnO and $ZnFe_2O_4$.

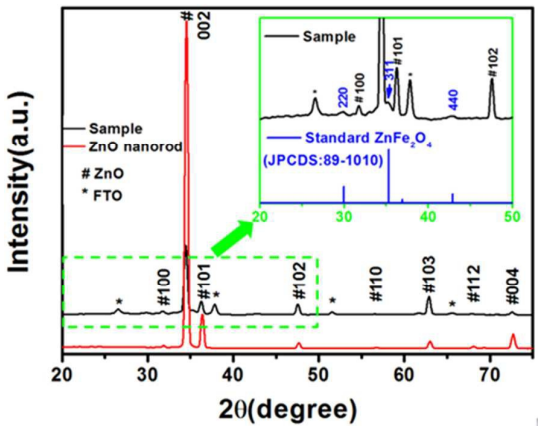

Fig. 2 XRD patterns of the $ZnO/ZnFe_2O_4$ hierarchical nanostructures (S2)

To further confirm the phases of $ZnFe_2O_4$ presented in the sample, the X-ray photoelectron spectroscopy was used to analyse the chemical bonding states of elements. Fig.3 is the typical XPS spectra of the $ZnO/ZnFe_2O_4$ heterostructure (S2 in Table1), where panel (a) is the survey spectrum and panels (b-d) are the high resolution binding energy spectra with fitting analysis for Zn, Fe and O, respectively. In $ZnFe_2O_4$, Fe and Zn atoms exist in the lattice with more than one chemical state (A-sites or B-sites), bringing about several different contributions with different binding energies in the X-ray photoelectron spectroscopy spectra.[26] Fig. 3b shows the detailed analysis of the Zn $2p_{3/2}$ peak. The main peak at 1021.5 eV is consistant with the X-ray photoelectron spectroscopy recorded for the standard $ZnFe_2O_4$ materials.[27] Hence we assume that the peak is related to the Zn ions inzinc ferrite. The other peak at 1021.8 eV should be due to ZnO. Fig. 3c shows the Fe 2p peaks at binding energies of 711.5 and 725.2 eV, with a shakeup satellite at 719.5 eV, which are characteristic of Fe^{3+} state in the cubic spinel $ZnFe_2O_4$ phase. [28] As shown in Fig. 3d, the O 1s spectrum shows a broad peak which is fitted by two peaks at binding energies of 530 and 531.6 eV. The peaks at 530.0 eV correspond to lattice oxygen linked to $ZnO/ZnFe_2O_4$, and the other peak at around 531.6eV ascribed to the the oxygen in the OH^- or H_2O absorbed on the sample surface. [29- 30]

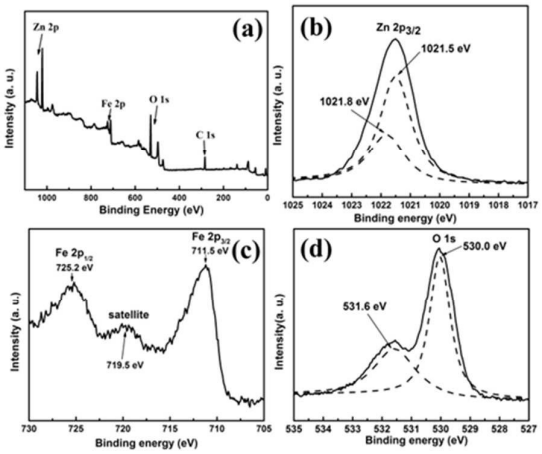

Fig. 3 XPS spectra of the $ZnO/ZnFe_2O_4$ nanoforest (S2): (a) survey of the sample, (b) Zn 2p, (c) Fe 2p, and (d) O 1s.

To get detailed structure of $ZnO/ZnFe_2O_4$ hierarchical composites, the TEM and HRTEM observation was further conducted. A typical TEM image (Fig. 4a) shows a branch of the $ZnO/ZnFe_2O_4$ nanoforest. The diameter of the nanorod was about 210-315nm, which was much smaller than primary ZnO nanorods. The enlarged TEM observation of a single branch (Fig. 4b) shows that some nanosheets were wrapped on the nanorod tightly. The HRTEM of the red square area in Fig.4b was shown in Fig. 4c. Fig. 4(d-f) shows the HRTEM of $ZnO/ZnFe_2O_4$ composites in different areas (marked by blue square) of Fig. 4c. The lattice fringe spacing in the nanosheet was observed to be 0.48nm and 0.25nm, corresponding to the (111) and (311) plane of $ZnFe_2O_4$. Figure 4f gives a lattice fringe of about 0.52 nm, corresponding to the (0001) fringes perpendicular to the growth direction of ZnO nanorod[31]. Fig. 4g shows the TEM image of the two nanorods. And the TEM elemental mapping was conducted to clearly identify the spatial distributions of Zn and Fe in the hierarchical structure

(Fig. 4h and Fig.4i). In the inner region, the signals of Zn were strongly detected, while the Fe signals were barely visible. In contrast, the Fe signals were dominant in the outer region, while a small amount of Zn signals were present.

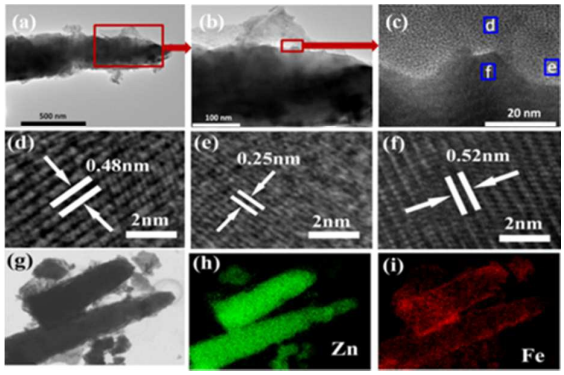

Fig. 4 (a) Typical TEM of the $ZnO/ZnFe_2O_4$ hierarchical nanostructures. (b) is the enlarged TEM images and (c) is HRTEM images of the red square area in (b). (d-f) is Higher magnification HRTEM images of several blue square areas in (c). Fig.(g-i) is the TEM image and the corresponding elemental mapping images.

The concentration of the $FeSO_4$ precursor plays an important role in controlling the final morphology of the hierarchical nanostructures. Fig. 5(a-d) shows the SEM images of the $ZnO/ZnFe_2O_4$ hierarchical nanostructures with the concentrations of ferrous sulfate solution ranging from 0.1 M to 0.8 M (S1-S4). After immersing in 0.1 M $FeSO_4$ solution for 30min, the surface of initial ZnO nanorods become rough and the sheet-like shapes could be detected (Fig. 5a). Once the concentration of $FeSO_4$ was increased to 0.2 M, the diameter of nanorods decreased and the product exhibited a forest-like morphology (Fig. 5b). As the concentration of $FeSO_4$ was 0.4M, the ZnO nanorods were further dissolved by H^+ produced from $FeSO_4$ hydrolysis. Then the nanorods disappeared but nanosheets were observed as the concentration reached 0.8M (Fig. 5d), indicating a significant change in morphology.

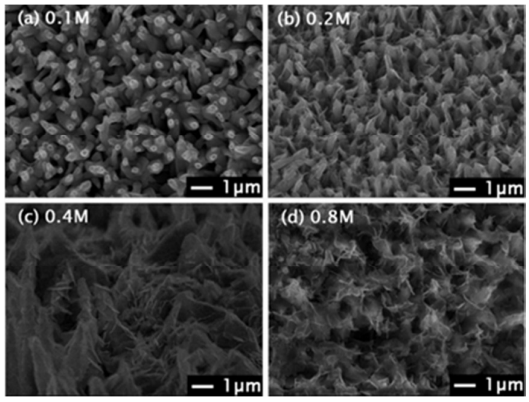

Fig. 5 SEM images of $ZnO/ZnFe_2O_4$ nanostructured films fabricated with different $FeSO_4$ concentrations for 30min. (a) 0.1M(S1), (b) 0.2M (S2), (c) 0.4M (S3), (d) 0.8M (S4).

In order to have a closer inspection of the evolution processes of hierarchical $ZnO/ZnFe_2O_4$ nanostructures, a series of time-dependent experiments were carried out. Fig. 6(a-d) show the SEM images of the products obtained after dipping in 0.2M ferrous sulfate solution for different time ranging from 5min to 30min. The insets of Fig. 6 are the sample picture corresponding to the SEM images, which clearly reveals the gradual change of the color. For the sample having reacted for 5min, the diameter of ZnO nanorods hardly changed and small amount of nanosheets were observed (Fig. 6a). When the reaction proceeded to 10 min, the diameter of nanorods greatly decreased, and plenty of nanosheets were observed around the nanorods (Fig. 6b). As the reaction was prolonged to 20 min, the nanosheets became smaller and covered on the surface of ZnO nanorods (Fig. 6c). For time closed to 30min, high-yield and uniform nanoforest structures could be produced (Fig. 6d).

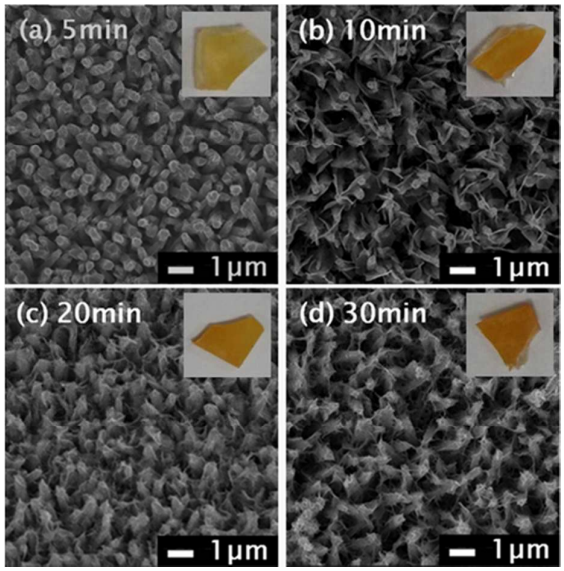

Fig. 6 SEM images of $ZnO/ZnFe_2O_4$ nanostructured films fabricated after the immersion in 0.2M ferrous sulfate solution for different time, (a) 5min (S5) (b) 10min (S6) (c) 20min (S7) (d) 30min (S2). The inset is the photograph of the corresponding samples.

On the basis of the results stated above, the formation process of the hierarchical $ZnO/ZnFe_2O_4$ nanostructures is proposed. As mentioned above, the surface of ZnO nanorods is coated with $ZnFe_2O_4$ nanosheets tightly, and the diameter of ZnO nanorods decreases from about 500 nm to 210 nm, indicating that the nanorods were partly dissolved during the immersion period. At the initial immersion stage, $FeSO_4$ easily hydrolyzes to form $Fe(OH)_2$ colloid and H^+ and further oxidized to FeOOH by oxygen in water. In the meantime, ZnO nanorods are dissolved under the H^+ atmosphere.[32] The consumption of proton in turn accelerates continuous hydrolysis of $FeSO_4$ in the immediate vicinity of ZnOnanorods. Besides, Zn^{2+} can also hydrolyze to form hydrated $Zn(OH)_2$ species. As a result, the precipitation of FeOOH and $Zn(OH)_2$ occurs preferentially on the surface of ZnO nanorods, resulting in the formation of

$Zn(OH)_2$–FeOOH nuclei. As increasing the immersion time, the $Zn(OH)_2$–FeOOH nuclei grow into nanosheets, leading to construction of hierarchical architecture. After further oxidation in air and subsequent calcination at 500°C, hierarchical ZnO/$ZnFe_2O_4$ nanoforest were finally constructed. The proposed reaction can be illustrated as follows:

$$4Fe^{2+} + 6H_2O + O_2 \rightarrow 4FeOOH + 8H^+ \quad (1)$$

$$ZnO + 2H^+ \rightarrow Zn^{2+} + H_2O \quad (2)$$

$$Zn^{2+} + 2H_2O \rightarrow Zn(OH)_2 + 2H^+ \quad (3)$$

$$2FeOOH + Zn(OH)_2 \xrightarrow{500℃} ZnFe_2O_4 + 2H_2O \quad (4)$$

It is well known that ZnO and $ZnFe_2O_4$ are two important kinds of sensing materials. The gas-sensing performance of a hetero-structure consisting of two metal oxides might be more excellent compared to pure ZnO nanorods. For comparison, two gas sensors based on the ZnO nanorods and ZnO/$ZnFe_2O_4$ hierarchical nanostructure were fabricated. Fig.7a shows the responses of the sensor based on the ZnO nanorods and ZnO/$ZnFe_2O_4$. As expected, the sensor using ZnO/$ZnFe_2O_4$ hierarchical nanostructure clearly exhibited enhanced response to ethanol compared with ZnO nanorods. Moreover, the ZnO/$ZnFe_2O_4$ sensor showed little responses to acetone, and almost insensitive to toluene, methanol and C_2H_4. The highest response of the sensor based on ZnO/$ZnFe_2O_4$ was about 10 to 100ppm ethanol, which is much higher than other gases, which indicated that the sensor showed selectivity to ethanol as opposed to other gases. Fig. 7b shows the responses of two sensors to 100 ppm ethanol at operating temperature from 225 °C to 325 °C. Obviously, the responses of two sensors were both dependent on the operating temperature. At various temperatures, the response of sensor based on ZnO/$ZnFe_2O_4$ hierarchical nanostructure to ethanol was higher than that of ZnO nanorods. Each sensor had an optimal operating temperature, at which the response value obtained the maximum.

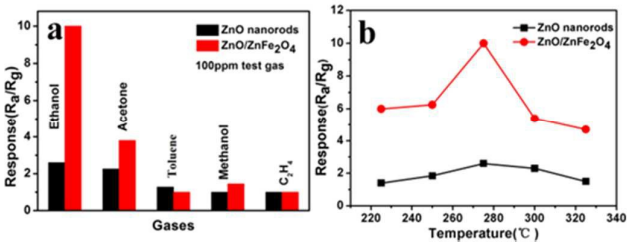

Fig. 7 (a) Responses of sensors based on the ZnO nanorods and ZnO/$ZnFe_2O_4$ (S2) toward various gases at 275 °C. (b) Responses of two sensors to 100 ppm ethanol as a function of operating temperature.

The dynamic response-recovery curves of the two sensors to 100 ppm ethanol at 275°C were shown in Fig. 8. The results showed that the response of the sensor based on ZnO/$ZnFe_2O_4$ hierarchical nanostructure was almost 4 times higher than that of sensor using ZnO nanorods. It is noteworthy that the ZnO/$ZnFe_2O_4$ sensor had a quicker response and recovery than ZnO sensor.

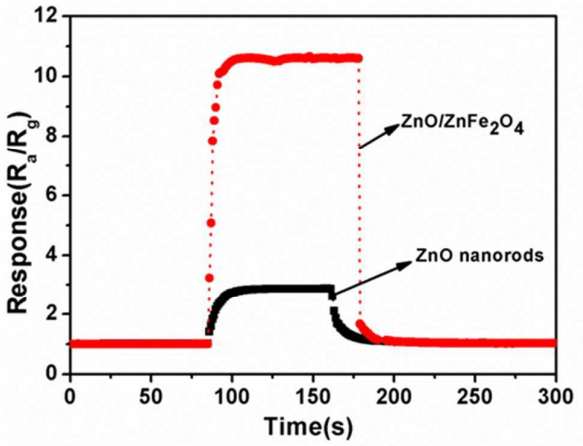

Fig. 8 Response transients of the sensors based on the ZnO nanorods and ZnO/$ZnFe_2O_4$ (S2) toward 100 ppm ethanol at 275°C

The significant improvement in gas-sensing property on ZnO/$ZnFe_2O_4$ hierarchical composites is likely to be the result of two factors. First, due to $ZnFe_2O_4$ and ZnO are important sensing materials, the synergetic effect of different gas sensing materials is considered. This effect has been observed in other hierarchical composites. [33-34] Second, the heterojunction forms at the interface between $ZnFe_2O_4$ and ZnO, as shown in SEM and TEM. Thus, electron depletion layer would be generated at the interface of two metal oxides, which is caused by their different band gaps and work functions.[35-36] Therefore, electrons will transfer between the conduction bands of the two oxides to equalize the Fermi energy levels. Hence, an electron depletion layer is formed at the interface of the two metal oxides. When the ZnO/$ZnFe_2O_4$ sensor was exposed to the air, O_2 molecules can easily adsorb on the surface of $ZnFe_2O_4$ and capture electrons from the conduction bands of $ZnFe_2O_4$ to be oxygen species (O^-, O^{2-}). The thickness electron depletion layer will further decrease due to the transfer of elections. As a result, the measured resistant of composite will increase because of the low concentration of free elections. When the sensor was exposed to a reductive gas such as ethanol, surface reaction between the oxygen species and gas molecules can occur and release a higher amount of electrons trapped in the ionized oxygen species.[36] Therefore, there is a greater drop of resistance in the case of ZnO/$ZnFe_2O_4$ sensor, resulting in an improved sensor response.
in text of the article should appear here with headings as appropriate.

Conclusions

In summary, hybrid ZnO/$ZnFe_2O_4$ nanoforest was successfully synthesized via a simple two-step method, which involved

immersing ZnO nanorod arrays in 0.2 M aqueous solution of ferrous sulfate and subsequent calcinations at 500℃. The ZnO template was partly dissolved in the immersion process and the forest-like architecture was generated. The time-dependent morphology evolution of $ZnO/ZnFe_2O_4$ samples was studied in detail, and a possible growth mechanism was proposed on the basis of experiment results. The resulting $ZnO/ZnFe_2O_4$ nanoforest displayed enhanced gas-sensing properties compared to the original ZnO nanorods. The excellent performance of $ZnO/ZnFe_2O_4$ films is attributed to the unique architecture and the formation of the heterojunction. Besides, this work suggests a simple method of making hetero-junctions for gas sensors.

Acknowledgements

This work was supported by NSFC (61474057, 61134010 and 61327804) and Program for Chang Jiang Scholars and Innovative Research Team in University (No. IRT13018), National High-Tech Research and Development Program of China (863 Program, No. 2014AA06A505) and the project development plan of science and technology of Jilin Province (20130521009JH).

References

1 H. L. Yu, L. Li, X. M. Gao, Y. Zhang, F. N. Meng, T. S. Wang, G. Xiao, Y. J. Chen and C. L. Zhu, *Sens. Actuators, B,* 2012,**171/172**, 679–685.
2 T. Jinkawa, G. Sakai, J. Tamaki, N. Miura, N. Yamazoe, *J J. Mol. Catal. A: Chem.,* 2000, **155**, 193–200.
3 D. W. Chu, Y. P. Zeng, D. L. Jiang, Y. Masuda, *Sens. Actuators, B,*2009, **137,** 630–636.
4 M. T. Niu, F. Huang, L. F. Cui, P. Huang, Y. L. Yu, Y. S. Wang, *ACS Nano,* 2010, **4**, 681–688.
5 W. W. Zhou, C. W. Cheng, J. P. Liu, Y. Y. Tay, J. Jiang, X. T. Jia, J. X. Zhang, H. Gong, H. H. Hng, T. Yu, H. J. Fan, *Adv. Funct.Mater.*, 2011, **21**, 2439–2445.
6 L. M. Qin, Q. Zhu, G. R. Li, F. T. Liu and Q. M. Pan, *J. Mater. Chem.*, 2012, **22**, 7544–7550.
7 Y. Liu, L. Yu, Y. Hu, C. Guo, F. Zhang and X. W. Lou, *Nanoscale,* 2012, **4**, 183-187.
8 Y. V. Kanetia, Q. M. D. Zakariaa, Z. J. Zhang, C. Y. Chena, J. Yueb, M. Liua, X. C. Jiang, and A. Yua, *J. Mater. Chem. A*, 2014, **2**, 13283-13292
9 J. Kang, Q. Kuang, Z.-X. Xie and L.-S. Zheng, *J. Phys. Chem. C*, 2011, **115**, 7874-7879.
10 P. Sun, Y. X. Cai, S. S. Du, X. M. Xu, L. You, J. Ma, F. M. Liu, X. S. Liang, Y. F. Sun and G. Y. Lu, *Sens. Actuators, B,*2013,**182**, 336–343.
11 S. H. Hwang, J. Song, Y. Jung, O. Y. Kweon, H. Song and J. Jang, *Chem. Commun.,*2011, **47**, 9164-9166.
12 J. Y. Lao, J. G. Wen and Z. F. Ren, *Nano. Lett.*, 2002, **2,** 1287–1291.
13 L. M. Huang and H. Q. Fan, *Sens. Actuators, B,* 2012, **171/172**,1257– 1263
14 Z. Zhang, C. Shao, X. Li, L. Zhang, H. Xue, C. Wang and Y. Liu, *J. Phys. Chem. C*, 2010, **114**, 7920-7925.
15 Y. X. Cai, X. W. Li, Y. Liu, S. S. Du, P. F. Cheng, F. M. Liu, K. Shimanoe, N. Yamazoe and G. Y. Lu, *CrystEngcomm*, 2014, **16,** 6135-6140.
16 H. S. Qian, Y. Hu, Z. Q. Li, X. Y. Yang, L. C. Li, X. T. Zhang and R. Xu , *J. Phys. Chem. C,* 2010**, 114***,* 17455-17459.
17 D. D. Qin and C. L. Tao, *RSC Adv.*, 2014, **4,** 16968–16972.
18 G.H. Kuo, H. PaulWang, H. H. Hsu, JamesWang, Y. M. Chiu, C.-J. G. Jou, *J Nanomater.*, 2009, **2009**, 4.
19 L. L. Li, Y. Chu, Y. Liu and L. H. Dong, *J. Phys. Chem. C*, 2007, **111**, 2123–2127.
20 T. Cheng, Z. Y. Fang, Q. X. Hu, K. D. Han, X. Z. Yang and Y. J. Zhang, *Catalysis Communications*, 2007, **8**, 1167–1171.
21 M. N. Rumyantseva, V. V. Kovalenko, A. M. Gaskov, T. Pagnier, D. Machon and J. Arbiol, J. R. Morante, *Sens. Actuators, B,*2005, **109**, 64–74.
22 C. H. Ong, J. H. Wang, H. Gong and H. S. O. Chan, *Int J Mod Phys B,***2002**, 16, 314–321.
23 P. Singh, A. Kaushal and D. Kaur, *J Alloy Compd,* 2009, **471**, 11–15.
24 Y. X. Cai, X. W. Li, P. Sun, B. Wang, F. M. Liu, P. F. Cheng, S. S. Du and G. Y. Lu, *Mater. Lett.*, 2013, **112**, 36 –38.
25 F. Pan, Y. Guo, F. F. Cheng, T. Fa, and S. D. Yao, *Chin. Phys. B*, 2011, **20**, 127501.
26 A. A. Tahir and K. G. Upul Wijayantha, *J. Photochem. Photobio. A: Chem,* 2010, **216**, 119.
27 A. Zaleska, P. G´orska, J. W. Sobczak and J. Hupka, *Appl. Catal., B,* 2007, **76**, 1–8.
28 J. F. Marco, J. R. Gancedo, M. Gracia, J. L. Gautier, E. Rios and F. J. Berry, *J. Solid State Chem.*, 2000, **153**, 74.
29 A. C. Tavares, M. I. da Silva Pereira, M. H. Mendon¸ca, M. R. Nunes, F. M. Costa and C. M. S´a, *J. Electroanal. Chem.*, 1998, **449**, 91.
30 J. P. Liu, Y. Y. Li, H. J. Fan, Z. H. Zhu, J. Jiang, R. M. Ding,Y. Y. Hu and X. T. Huang, *Chem. Mater.,* 2010, **22,** 212–217.
31 G. Z. Shen, Y. S. Bando, B. D. Liu, D. Golberg and C.-J. Lee, *Adv. Funct. Mater.* 2006, 16, 410–416.
32 Y. J. Chen, C. L. Zhu, X. L. Shi, M. S. Cao and H. B. Jin, *Nanotechnology*, 2008, **19** ,205603.
33 C. L. Zhu, Y. J. Chen, R. X. Wang, L. J. Wang, M. S. Cao and X. L. Shi, *Sens. Actuators, B*, 2009, **140,** 185–189.
34 J. Zhang, X. Liu, L. Wang, T. Yang, X. Guo, S. Wu, S. Wang and S. Zhang, *Nanotechnology*, 2011, **22**, 185501.
35 P. Sun, X. Zhou, C. Wang, K. Shimanoe, G. Y. Lu and N. Yamazoe, *J. Mater. Chem. A*, 2014, **2,** 1302-1308
36 N. Yamazoe, J. Fuchigami, M. Kishikawa and T. Seiyama, *Surf. Sci.*, 1979, **86**, 335–344.